



## 填表说明

一、本报告中相关的技术或数据如涉及知识产权保护、军工项目保密等内容，请作脱密处理。

二、请用宋体小四字号撰写本报告，可另行附页或增加页数，A4纸双面打印。

三、表中所涉及的签名都必须用蓝、黑色墨水笔，亲笔签名或签字章，不可以打印代替。

四、同行专家业内评价意见书编号由工程师学院填写，编号规则为：年份4位+申报工程师职称专业类别(领域)4位+流水号3位，共11位。

## 一、个人申报

(一) 基本情况【围绕《浙江工程师学院(浙江大学工程师学院)工程类专业学位研究生工程师职称评审参考指标》，结合该专业类别(领域)工程师职称评审相关标准，举例说明】

### 1. 对本专业基础理论知识和专业技术知识掌握情况(不少于200字)

1. 基础理论深度：扎实掌握化工热力学(相平衡计算、流体PVT性质预测)、反应工程(反应动力学分析、反应器选型设计)、传递过程原理(三传一反机理)，并能将理论应用于工艺流程优化。
2. 专业技术应用：精通化工过程模拟(Aspen Plus/HYSYS稳态优化、COMSOL多物理场仿真)
3. 掌握高端分离技术(分子筛吸附、膜分离集成)，设计溶剂回收系统使医药中间体生产成本下降
4. 熟悉催化剂开发与表征(BET、TPR/TPD测试)，参与的燃料电池活性催化剂的合成。

持续学习：持续学习《工程技术创新前言》《产业技术发展前沿》《绿色化工与生物催化前沿》等前沿化工课程

### 2. 工程实践的经历(不少于200字)

进行了燃料电池汽车以及燃料电池行业的市场调研、文献查询，分析了中国国内燃料电池汽车及燃料电池行业的市场行情、发展趋势及产品情况，了解了当前市场的主要燃料电池汽车及燃料电池代表企业的情况。对江苏海四达电源股份有限公司的产业格局、企业文化、发展历程以进行了深入了解，前往电池等零部件生产车间进行了相关的参观、了解和体验。搜集高温质子交换膜市场目前存在的问题，对高温膜的改性进行研究，了解市场流通的主要质子交换膜类型及性质，研究质子交换膜所存在的问题，设计实验，开展关于质子交换膜改性的相关实验研究，并对原膜进行简要的对比。总结实践工作，撰写总结报告。

### 3. 在实际工作中综合运用所学知识解决复杂工程问题的案例(不少于1000字)

在开发新一代高温质子交换膜燃料电池的核心组件过程中，我直面了制约行业发展的三重技术瓶颈：首先，在80-180℃无水质子传导环境下，增塑剂磷酸(PA)的严重流失导致传统OPBI膜运行200小时后电导率衰减超40%，而提升PA负载量又引发膜溶胀，使机械强度从45MPa骤降至危险临界值28MPa；其次，阴极侧产生的·OH自由基持续攻击聚合物链，使膜材料在Fenton加速测试中72小时即断裂失效；更棘手的是，当引入无机填料改善传导性时，15%负载量即出现填料团聚，反而阻断质子通道使电导率下降10%。这些矛盾本质是材料化学、传质动力学与机械强度学的多学科耦合难题，必须构建跨尺度解决方案。

针对上述挑战，我主导设计了系统性技术路径。在分子尺度上，基于配位化学原理创新提出联吡啶基共价有机框架(TpBPy-COF)增强策略：其吡啶环氮原子孤对电子可与PA的P=O键形成强Lewis酸碱对，理论结合能计算>120 kJ/mol，从根本上抑制PA流失。具体实施中，通过优化溶剂热合成工艺——将5,5'-二氨基-2,2'-联吡啶与三甲酰基间苯三酚在均三甲苯/二氧六环/6M醋酸混合体系(体积比5:5:1)中120℃反应5天，再经THF索氏提取24小时纯化，获得比表面积达980 m<sup>2</sup>/g、孔径分布2.8-3.5nm(精准匹配PA分子尺寸)的COF材料，产率提升至72.4%。在复合膜制备环节，采用500W功率超声分散8小时使COF粒径≤200nm，结合80℃→100℃阶梯升温浇铸工艺消除内应力，并创新性在COF表面接枝OPBI相容链段，原子力显微镜(AFM)相位成像证实界面能降低35%

，成功构建连续质子通道（小角X射线散射显示特征离子簇峰 $q=0.8\text{ nm}^{-1}$ ）。

在诊断技术层面，传统毫米级电极在 $180^{\circ}\text{C}$ 下背景噪声高达mA级，无法解析真实传质行为。为此我自主开发超微电极电化学平台：采用激光拉制法制备直径 $10\text{ }\mu\text{m}$ 铂微盘电极（SEM验证边缘精度 $\pm 0.2\text{ }\mu\text{m}$ ），使响应电流降至nA级；设计双层 $\mu\text{-metal}$ 合金电磁屏蔽舱实现 $>60\text{dB}$ 干扰衰减，结合锁相放大技术建立高温工况原位测试能力。基于此平台，首次通过取样计时电流法（SCV）获取高信噪比曲线，并运用Cottrell方程逆向求解扩散系数（ $D=2.1\times 10^{-9}\text{ m}^2/\text{s}$ ，相对标准偏差 $<3\%$ ），该数据指导优化粘结剂孔隙率至35%，显著提升氧气传质效率。

工程验证阶段开展多维度严苛测试：热重分析（TGA）显示5%失重温度达 $320^{\circ}\text{C}$ ，满足 $200^{\circ}\text{C}$ 长期运行需求； $80^{\circ}\text{C}$

Fenton试剂中浸泡144小时后，膜断裂伸长率保持率 $>85\%$ ，预示寿命从3000小时延长至8000小时；表面粗糙度仅 $8.2\text{nm}$ （AFM），证实无宏观相分离。最终性能数据展现突破性提升： $180^{\circ}\text{C}$ 电导率达 $0.12\text{ S/cm}$ （较传统膜+140%，超越BASF Celtec® P1000商用膜33%），PA保持率89%，拉伸强度 $51\text{ MPa}$ ，峰值功率密度 $0.41\text{ W/cm}^2$ ，更实现 $-40^{\circ}\text{C}$ 冷启动（突破车规级门槛）。

该成果已产生显著工程价值：COF原料成本控制在 $<\$50/\text{g}$ （仅为商用Pt/C催化剂一半），推动高温膜降价32%；构建的微电极测试法，检测效率提升300%；项目实施中，我主导突破20%负载量阈值（电导率 $0.14\text{ S/cm}$ 未衰减）、建成国内首套pA级高温微电极平台、将膜缺陷率从12%降至0.3%，彰显从分子设计到系统集成的复杂工程问题解决能力。

本案例成功破解“传导-强度-寿命”不可能三角，理论层面融合配位化学与逾渗理论，技术层面填补国内极限工况检测空白，工程层面赋能新能源及9981领域，完全契合工程师职称评审对技术创新性与产业贡献度的核心要求。

(二) 取得的业绩(代表作)【限填3项, 须提交证明原件(包括发表的论文、出版的著作、专利证书、获奖证书、科技项目立项文件或合同、企业证明等)供核实, 并提供复印件一份】

1. 公开成果代表作【论文发表、专利成果、软件著作权、标准规范与行业工法制定、著作编写、科技成果获奖、学位论文等】

成果名称	成果类别 [含论文、授权专利(含发明专利申请)、软件著作权、标准、工法、著作、获奖、学位论文等]	发表时间/授权或申请时间等	刊物名称/专利授权或申请号等	本人排名/总人数	备注
Enhancement of Mass Transport in Catalyst Layers of HT-PEMFC with Tetrafluorophenyl Phosphonic Acid Binder	权威期刊	2024年06月06日	Chemistry An Asian Journal	1/6	

2. 其他代表作【主持或参与的课题研究项目、科技成果应用转化推广、企业技术难题解决方案、自主研发设计的产品或样机、技术报告、设计图纸、软课题研究报告、可行性研究报告、规划设计方案、施工或调试报告、工程实验、技术培训教材、推动行业发展中发挥的作用及取得的经济社会效益等】

(三) 在校期间课程、专业实践训练及学位论文相关情况

课程成绩情况	按课程学分核算的平均成绩： 83 分
专业实践训练时间及考核情况(具有三年及以上工作经历的不作要求)	累计时间： 1 年(要求1年及以上) 考核成绩： 83 分

**本人承诺**

个人声明：本人上述所填资料均为真实有效，如有虚假，愿承担一切责任，特此声明！

申报人签名：马壮



浙江大学研究生院  
攻读硕士学位研究生成绩表

学号: 22260437	姓名: 马壮	性别: 男	学院: 工程师学院	专业: 材料与化工	学制: 2.5年						
毕业时最低应获: 29.0学分		已获得: 31.0学分		入学年月: 2022-09	毕业年月:						
学位证书号:			毕业证书号:			授予学位:					
学习时间	课程名称	备注	学分	成绩	课程性质	学习时间	课程名称	备注	学分	成绩	课程性质
2022-2023学年秋季学期	创新设计方法		2.0	通过	专业选修课	2022-2023学年春季学期	材料加工技术		2.0	80	专业学位课
2022-2023学年秋季学期	工程技术创新前沿		1.5	86	专业学位课	2022-2023学年春季学期	新时代中国特色社会主义思想理论与实践		2.0	75	公共学位课
2022-2023学年秋季学期	工程伦理		2.0	84	公共学位课	2022-2023学年春季学期	优化理论基础		2.0	81	专业选修课
2022-2023学年冬季学期	膜技术与工程		2.0	90	专业学位课	2022-2023学年春季学期	研究生论文写作指导		1.0	89	专业学位课
2022-2023学年冬季学期	智慧能源系统工程		2.0	87	专业学位课	2022-2023学年春季学期	自然辩证法概论		1.0	82	公共学位课
2022-2023学年冬季学期	产业技术发展前沿		1.5	88	专业学位课	2022-2023学年夏季学期	研究生英语基础技能		1.0	77	公共学位课
2022-2023学年冬季学期	聚合物加工原理与分析方法		2.0	81	专业选修课	2022-2023学年春夏学期	高阶工程认知实践		3.0	78	专业学位课
2022-2023学年秋冬学期	研究生英语		2.0	87	公共学位课		硕士生读书报告		2.0	通过	
2022-2023学年春季学期	绿色化工与生物催化前沿		2.0	89	专业学位课						

说明: 1. 研究生课程按三种方法计分: 百分制, 两级制 (通过、不通过), 五级制 (优、良、中、及格、不及格)。  
2. 备注中 "\*" 表示重修课程。

学院成绩校核章

成绩校核人: 张梦依

打印日期: 2025-06-03



# CHEMISTRY

---

## AN **ASIAN** JOURNAL

www.chemasianj.org

### Accepted Article

**Title:** Enhancement of Mass Transport in Catalyst Layers of HT-PEMFC with Tetrafluorophenyl Phosphonic Acid Binder

**Authors:** Zhuang Ma, Jianchun Niu, Shuomeng Zhang, Jialin Zhang, Shanfu Lu, and Qinggang He

This manuscript has been accepted after peer review and appears as an Accepted Article online prior to editing, proofing, and formal publication of the final Version of Record (VoR). The VoR will be published online in Early View as soon as possible and may be different to this Accepted Article as a result of editing. Readers should obtain the VoR from the journal website shown below when it is published to ensure accuracy of information. The authors are responsible for the content of this Accepted Article.

**To be cited as:** *Chem. Asian J.* **2024**, e202400662

**Link to VoR:** <https://doi.org/10.1002/asia.202400662>

A Journal of



WILEY-VCH

# Enhancement of Mass Transport in Catalyst Layers of HT-PEMFC with Tetrafluorophenyl Phosphonic Acid Binder

Zhuang Ma <sup>a</sup>, Jianchun Niu <sup>a</sup>, Shuomeng Zhang <sup>a</sup>, Jialin Zhang <sup>b</sup>, Shanfu Lu <sup>b</sup>, Qinggang He <sup>a,\*</sup>

---

[a] Z. Ma, J. Niu, S. Zhang, Dr. Q. G. He

College of Chemical and Biological Engineering

Zhejiang University

Hangzhou, Zhejiang, 310027, China

E-mail: qghe@zju.edu.cn (Q. He)

[b] J. Zhang, Prof. S. F. Lu

Beijing Key Laboratory of Bioinspired Energy Materials and Devices, School of Energy and Power Engineering,

Beihang University

Beijing, 100191, China

Supporting information for this article is given via a link at the end of the document.

## Abstract

The design and development of new and efficient catalyst binder materials are important for improving cell performance in high-temperature proton-exchange membrane fuel cells (HT-PEMFCs). In this study, a series of tetrafluorophenyl phosphonic acid-based binder materials (PF-y-P,  $y = 1, 0.83, \text{ and } 0.67$ ) with rigid structures and controllable degrees of phosphonation were prepared and used in HT-PEMFCs using the ultra-strong acid-catalyzed Friedel–Crafts reaction and the combined Michaelis–Arbuzov reaction. The samples exhibited high stability, low water uptake, superior proton conductivity, and cell performance. In addition, the oxygen mass transport properties of the PF-1-P binder were investigated using high-temperature microelectrode electrochemical testing techniques. Compared with the phosphoric acid-doped polybenzimidazole (PBI) binder, the  $\text{O}_2$  solubility of PF-1-P binder material increased by 30% ( $5.36 \times 10^{-6} \text{ mol cm}^{-3}$ ) and the PF-1-P binder material exhibited better cell stability in HT-PEMFCs. After 10.5 h of discharge at a constant current of  $0.12 \text{ A cm}^{-2}$ , the MEA voltage decreased by 7.1% and 20.8% in case of the PF-1-P and PBI binders, respectively.

**Keywords:** High-temperature proton exchange membrane fuel cells; binder; tetrafluorophenyl phosphonic acid-based; oxygen mass transport; microelectrode

## 1. Introduction

Proton-exchange membrane fuel cells (PEMFCs) have been extensively investigated as emerging energy conversion devices<sup>[1]</sup>. According to the working temperature classification, proton-exchange membranes can be divided into low-temperature (50°C–80°C) and high-temperature proton-exchange membranes (100°C–180°C)<sup>[2]</sup>. The advantages of a high-temperature PEMFCs (HT-PEMFCs) are as follows: high tolerance to CO impurities at high temperatures, simple water and heat management systems, and high reaction and diffusion rates<sup>[3]</sup>. However, designing high-performance and high-applicability HT-PEMFCs remain a challenge<sup>[4]</sup>.

The catalyst layer (CL) in HT-PEMFC is the main site where the electrode redox reaction occurs and consists mainly of the binder and catalyst<sup>[5]</sup>. The binder, a thin layer of polymer electrolyte on the catalyst surface, is one of the basic components of HT-PEMFC, which mainly provides proton conduction<sup>[6]</sup> for electrochemical reactions and plays a key role in improving cell performance and reducing cost<sup>[7]</sup>. Currently, phosphoric acid (PA)-doped binder remains one of the widely used binder materials in HT-PEMFC<sup>[8]</sup>. PA acts as a carrier for conducting protons and plays a substantial role in promoting the formation of three-phase interfaces on the catalyst surface<sup>[9]</sup>. Maric et al<sup>[10]</sup> investigated the optimal<sup>[3f]</sup> polytetrafluoroethylene (PTFE) binder content in the CL of high-temperature H<sub>2</sub>/O<sub>2</sub> and H<sub>2</sub>/air proton-exchange membrane fuel cells using PA-doped pyridine aromatic polyethers as HT-PEM and showed that a high or low PTFE binder content in the CL is not conducive to improving cell performance. The right amount of PTFE can increase the pore structure of the CL and, to some extent,

facilitate proton transfer to the catalyst surface to form a three-phase interface for the catalytic reaction. However, when PA-doped binders are used in HT-PEMFCs, the active sites of the electrocatalysts may be covered by PA. In addition, the transport channels of reactants in CL are easily blocked by free PA, which affects the mass transport of oxygen in cathode CL and eventually leads to degradation of cell performance<sup>[11]</sup>.

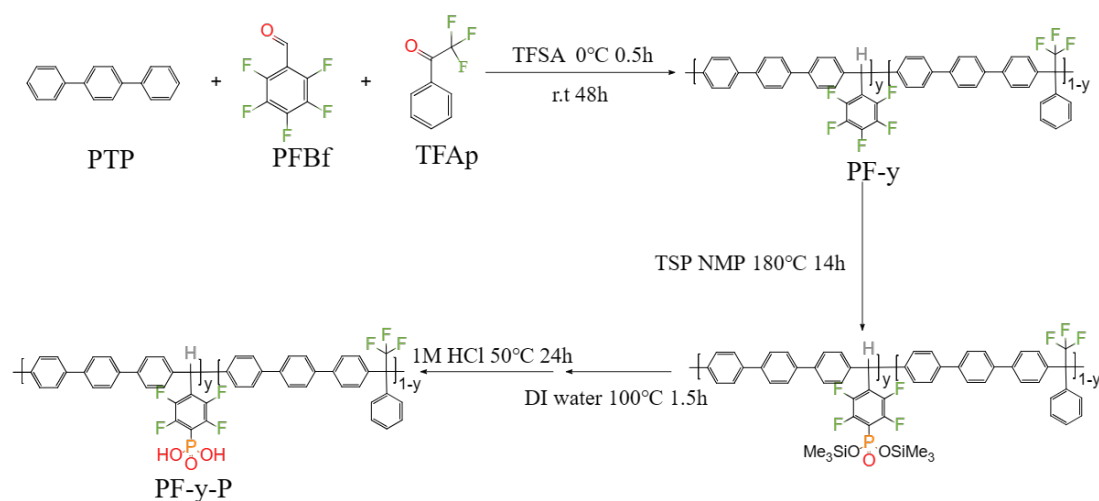
In our previous work, we investigated the effect of the content of binder PVP and PA in the CL on the mass transport of O<sub>2</sub> using a microelectrode electrochemical device and found that an increase in the content of PVP and the presence of a large amount of PA in the CL would lead to a decrease in the permeability of O<sub>2</sub>, which would result in a decrease in the performance of HT-PEMFC<sup>[12]</sup>. The diffusion coefficients, solubility, and permeability of O<sub>2</sub> with varying temperature were successfully obtained, indicating that the temperature has a considerable effect on O<sub>2</sub> mass transport in the CL of HT-PEMFCs. With increasing temperature, the diffusion coefficient of oxygen in the binder gradually increases, while the solubility first increases and then decreases. To further reveal the mechanism of oxygen mass transfer in binders, the diffusion process of O<sub>2</sub> molecules was described by a “sphere-cage” model based on the free volume theory and hard sphere model. In addition, a dual-mode model describing the dissolution process of O<sub>2</sub> molecules in PES-PVP-60 binder was established by fitting the experimental results<sup>[13]</sup>.

The chemical bonding of PA to polymers designed as phosphonic acid-based binder materials can effectively avoid a series of problems caused by doped PA<sup>[14]</sup>.

Atanasov et al<sup>[15]</sup> used the synthesized phosphonated poly(pentafluorostyrene) (PWN70) as a HT-PEMFC binder material and compared it with several PA-doped binders. The results show that although PWN70 is lower than most PA-doped binders in terms of both proton conductivity and film formability, the PWN70 ionomer not only exhibits excellent performance over a wide temperature range of 120°C–240°C but also has high cell stability of more than 550 h at 160°C and a high current of 0.6 A cm<sup>-2</sup>. However, phosphonic acid-based binder materials are prone to form phosphonic anhydride under high-temperature and low-humidity, and their proton conductivity decreases sharply, affecting the rate of the oxygen reduction reaction on the cathode side<sup>[14c]</sup>.

In this study, we report the preparation of a series of tetrafluorophenyl phosphonic acid-type polymeric materials with a controlled degree of phosphonation by Friedel-Crafts reaction catalyzed by a super acid (trifluoromethanesulfonic acid). Owing to the strong electron absorption of tetrafluorophenyl, the formation of anhydrides between neighboring phosphonic acid groups is effectively avoided or reduced. The stability, hydrophobicity, and electrical conductivity of these tetrafluorophenyl phosphonic acid-based binder materials were investigated. In particular, the oxygen mass transfer of the novel binder material was tested at 120°C using a microelectrode. The overall performance of the H<sub>2</sub>/O<sub>2</sub> HTPEMFC demonstrated that tetrafluorophenyl phosphonic acid-type polymeric materials are effective catalyst binder for a CL in high-temperature proton-exchange membrane fuel cell.

## 2. Results and Discussion



**Scheme 1.** Synthesis route of PF-y-P: Adjustment of the ratio of the polymerization monomers pTP, TFAP, and PFBf controls the degree of phosphonation

**Scheme 1** shows the synthetic route for PF-y-P ( $y$  is the Phosphonic acid group ratio). The formation of phosphonic anhydride was regulated by reducing the number of adjacent tetrafluorophenyl phosphonic acid groups by introducing TFAP. To obtain binders with different degrees of phosphonation, PF-y samples were prepared by regulating the ratio of polymeric monomers pTP, TFAP, and PFBf. The PF-y samples were polymerized under the catalytic effect of super acid TFSA. The molecular weights and polydispersity index of PF-y were evaluated using a gel permeation chromatograph (GPC shown in Table 1), and all the samples exhibited high molecular weights and a exhibited narrow molecular weight distribution<sup>[16]</sup>. Subsequently, phosphonate polymers (PF-1-P, PF-0.83-P, and PF-0.67-P) were obtained via Michaelis–Arbuzov reaction.

**Table 1** Molecular weight and polydispersity index of PF-y

PF-y	$M_n$ / (g mol <sup>-1</sup> )	$M_w$ / (g mol <sup>-1</sup> )	PDI
PF-1	25400	57300	2.26
PF-0.83	22800	46900	2.06
PF-0.67	20300	44300	2.18

Taking PF-1-P as an example, the analysis of the <sup>1</sup>H NMR spectra in Fig. 1(a) proves that the main chain of the PF-1-P polymer is the same as that of PF-1. In addition, the peak at a chemical shift of -155 ppm disappeared in the <sup>19</sup>F NMR spectrum (Fig. 1(b)) and the ratio of the integrated area of the two peaks between -130 ppm and -140 ppm is 1:1. This indicates that the functional group Fig. S1(a') in PF-1 is involved in the reaction, whereas the unreacted Fig. S1(b') and Fig. S1(c') are retained on the polymer, and the presence of only one <sup>31</sup>P NMR peak attributed to the tetrafluorophenyl phosphonic acid functional group in Fig. 1(c). Similarly, the <sup>1</sup>H NMR, <sup>19</sup>F NMR, and <sup>31</sup>P NMR spectra in Fig. 1 indicates the successful preparation of the PF-0.83-P and PF-0.67-P polymeric materials.

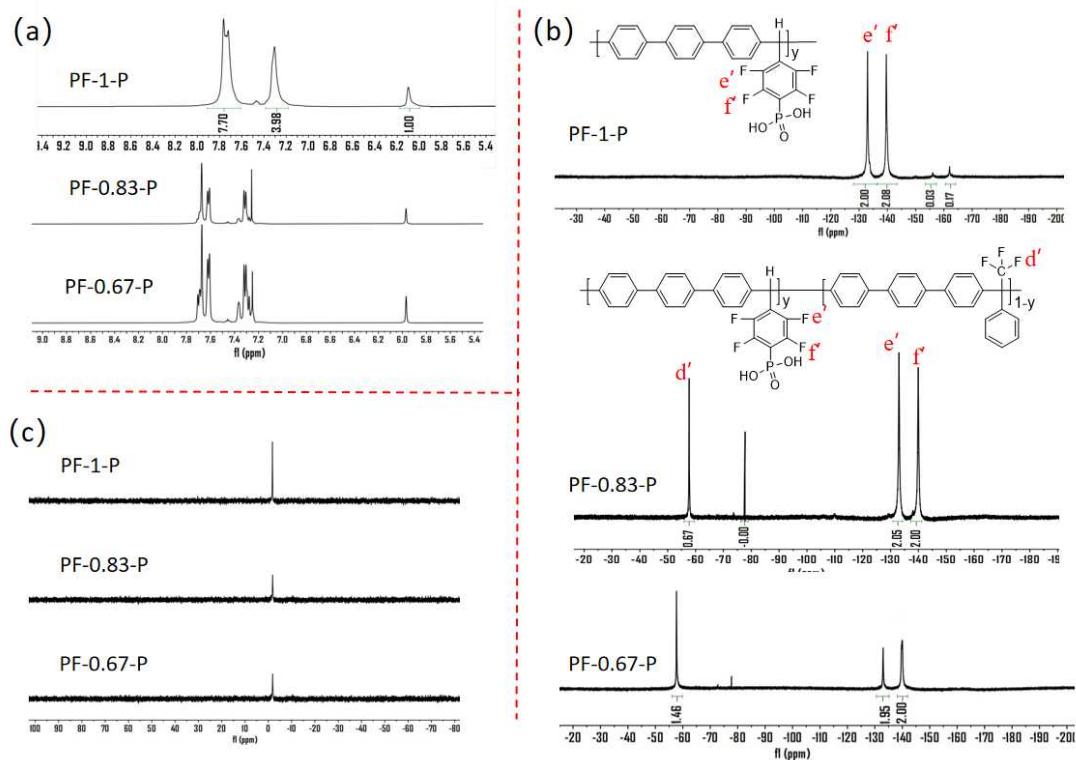


**Fig. 1.**  $^1\text{H}$  NMR,  $^{19}\text{F}$  NMR, and  $^{31}\text{P}$  NMR spectra of PF-y-P in  $\text{DMSO-d}_6$ : (a)  $^1\text{H}$  NMR, (b)  $^{19}\text{F}$  NMR, (c)  $^{31}\text{P}$  NMR

To investigate the thermal and chemical stability of PF-y-P binder materials suitable for HT-PEMFC operating temperatures, PF-y-P binder materials were subjected to NMR tests after being kept at  $250^\circ\text{C}$  for 2 h and Fenton's reagent immersion at  $80^\circ\text{C}$  for 12 h. Fig. S2 and S3 show that the  $^1\text{H}$  NMR,  $^{19}\text{F}$  NMR, and  $^{31}\text{P}$  NMR spectra of PF-1-P, PF-0.83-P, and PF-0.67-P binder materials show marginal differences compared with those before treatment.

The hydrophilic nature of the material can lead to “flooding” of the catalytic layer, as well as clogging of the secondary pores in the cathodic catalytic layer, thus affecting the oxygen transfer to the active center of the catalyst. Based on Eq. S(1) and Eq. S(2), Fig. 2 shows the water uptake (Fig. 2(a) and Table 2) and dimensional swelling (Fig.

2(b) and Table 3) of PF-y-P and PBI binder materials after water absorption to saturation in deionized water at 40°C, 60°C, 80°C, and 100°C, respectively. Water absorption increased with increasing temperature for both PF-y-P and PBI binders. Under the same temperature conditions, the water uptake of the materials from highest to lowest was PF-1-P, PBI, PF-0.83-P, and PF-0.67-P. This indicates that the increase in the functionalities of tetrafluorophenyl phosphonic acid may facilitate water uptake. Moreover, the water contact angle test (Fig. S4) showed that PF-1-P is more hydrophilic than PF-0.67-P, PF-0.83-P, and PBI.

Dimensional swelling ( $t_{sw}$ ) of the binder destroys the microstructure of the catalytic layer, thereby affecting the stability of the cell<sup>[17]</sup>. The dimensional swelling of the PF-y-P and PBI binder materials follows the same trend as their water uptake, i.e., the increase in the water content of both types of binder materials leads to an increase in their dimensional swelling as the temperature increases, but the change is small. In addition, the dimensional solubility of the material was also in the order of PF 1-P, PBI, PF-0.83-P, and PF-0.67-P from high to low, and the higher the degree of phosphonate acidification, the greater the dimensional swelling.

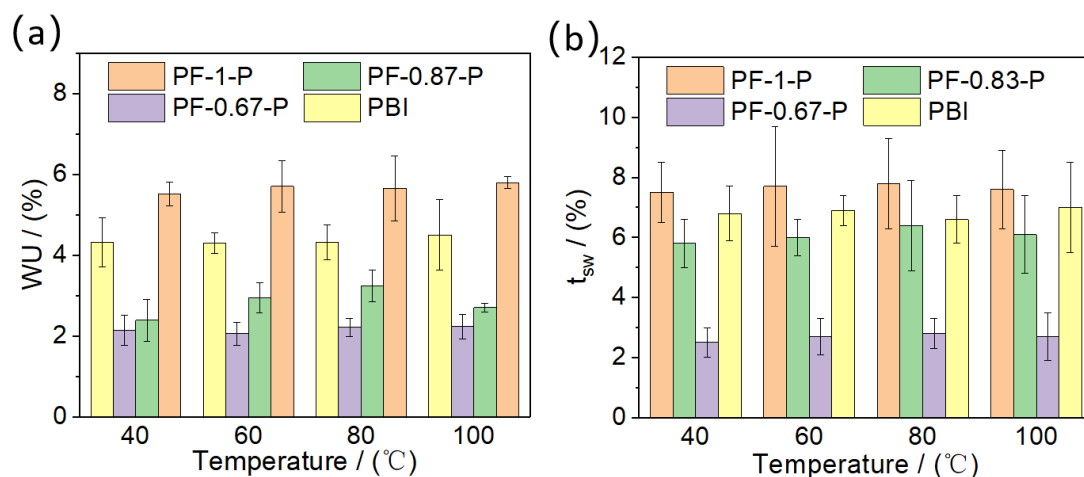


**Fig. 2.** Water uptake and swelling ratio of PF-y-P and PBI at 40°C–100°C: (a) water uptake, (b) swelling ratio

**Table 2** Water uptake(%) of PF-y-P and PBI

Temperature / (°C)	PF-1-P	PF-0.87-P	PF-0.67-P	PBI
100	5.799±0.138	2.699±0.115	2.236±0.306	4.500±0.874
80	5.652±0.808	3.239±0.394	2.211±0.224	4.318±0.427
60	5.701±0.633	2.951±0.376	2.060±0.284	4.295±0.253
40	5.505±0.296	2.390±0.517	2.136±0.378	4.317±0.599

**Table 3** Swelling ratio(%) of PF-y-P and PBI

Temperature/ (°C)	PF-1-P	PF-0.87-P	PF-0.67-P	PBI
40	7.5±1	5.8±0.8	2.5±0.5	6.8±0.9
60	7.7±2	6±0.6	2.7±0.6	6.9±0.5
80	7.8±1.5	6.4±1.5	2.8±0.5	6.6±0.8
100	7.6±1.5	6.1±1.3	2.7±0.8	7±1.5

To investigate the effect of the structure of tetrafluorophenylphosphonic acid on the proton conducting properties of the binder material, the ionic conductivity of PF-y-P was tested by electrochemical impedance spectroscopy (EIS). From the measured EIS Fig. S5(a–d), it is clear that the EIS plot contains two parts: the semicircular part in the high-frequency region and the diagonal part in the low-frequency region with an inclination angle of approximately 45°. Among them, the resistance of the binder material mainly depends on the semicircular part of the high-frequency region in the EIS, and the diagonal part of the low-frequency region is mainly due to the Warburg impedance caused by the control of material transfer<sup>[18]</sup>. The equivalent circuit shown in Fig. S5(e) is used for fitting to find the corresponding resistance. The corresponding proton conductivity is then calculated using Eq. S(3), and the proton transport activation

energy of the sample is further calculated using Eqs. S(4) (Arrhenius equation) and S(5)<sup>[16, 19]</sup>.

Fig. 3(a) shows that the proton conductivity of both PF-y-P binder materials increases with increasing temperature; this is due to the fact that the higher the temperature, the higher the activation energy of proton conduction using Eq. S(4) (Arrhenius equation). In combination with Fig. 3(a–b), the proton conductivity of the binder materials increases with increasing phosphonation, which is mainly because the PF-y-P binder materials need to rely only on the tetrafluorophenyl phosphonate group to transfer protons, and the higher degree of phosphonation is beneficial to increase the proton transport sites, and it is also easy to form proton transport channels between the phosphonates, which is beneficial to the proton “jump.”<sup>[20]</sup>

However, among the PF-y-P binder materials, the PF-1-P material reached the highest proton conductivity of  $5.06 \text{ mS cm}^{-1}$  at  $180^\circ\text{C}$ , which is lower than that of PBI at the same temperature by nearly  $51.06 \text{ mS cm}^{-1}$ . Despite the difference of an order of magnitude, it is not substantial in terms of fuel cell performance as shown below, suggesting that the conductivity of the binder is not a constraint on fuel cell performance and can be improved through structural optimization.

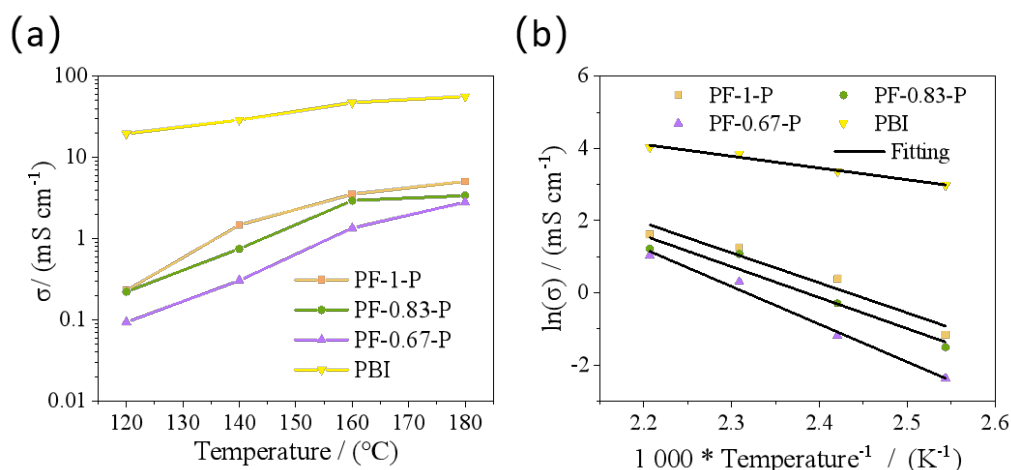


**Fig. 3.** PF-y-P and PBI binder: (a) proton conductivity versus temperature (120 $^{\circ}\text{C}$ –180 $^{\circ}\text{C}$ ); (b)

Arrhenius curve between proton conductivity and temperature ( $\ln(\sigma)$  vs  $1000T^{-1}$ )

Oxygen mass transfer is one of the main factors to achieve high-performance cathode CL, and the oxygen mass transfer properties of the binder material itself cannot be ignored. In this study, a microelectrode electrochemical system is built for the quantitative characterization of the  $\text{O}_2$  mass transport coefficients in a binder. In Fig. 4(a), cyclic voltammograms obtained in  $\text{N}_2$  and  $\text{O}_2$  atmospheres at a scan rate of 250  $\text{mV s}^{-1}$  were used to determine the ORR initial potential of 0.62 V by comparing the CV curves in  $\text{N}_2$  and  $\text{O}_2$  atmospheres. Then, potential step chronoamperometric (CA) measurements were performed in an oxygen environment from 0.62 V to -0.6 V to obtain Fig. 4(b). The I-t curves show the same trend at all different final potentials. The transient current I decreases rapidly with time and then slows down to a steady state. These curves intersect at 2 s, which suggests that the overpotential is large enough for the ORR to react in the  $\text{O}_2$  mass-transport-limiting mechanism. Therefore, we sampled the current I from the I-t curve at 2 s and plotted the sampled I versus  $V_f$  to obtain Fig.

4(c). The SCV curves in Fig. 4(c) are categorized into three cases: the kinetic or mixed kinetic regime, the diffusion control regime, and the H<sub>2</sub> evolution regime. Fig. 4(d-f) and Table 4 show the results of O<sub>2</sub> diffusion coefficient ( $D_{O_2}$ ), solubility ( $C_{O_2}$ ), and permeability ( $D_{O_2} * C_{O_2}$ ) of the PF-y-P class binder and PBI binder materials tested using the microelectrode technique at 120°C. More experimental details are reported in the supporting information (Fig.S7 – Fig.S11). From Fig. 4(d), the O<sub>2</sub> diffusion coefficient of PF-y-P-type binders gradually increases with decreasing phosphonation; this suggests that the free volume of the polymer increases as the degree of phosphonation decreases and that the change is rooted in the fact that the intermolecular forces between the tetrafluorophenyl phosphonic acid groups of the side chains are greater than those between the benzene rings (Fig. S6). According to the free volume theory<sup>[21]</sup> when O<sub>2</sub> molecules thermally vibrate to a specific position in the hole, the polymer chain segment at that position appears to be in torsion or relative motion. This provides a transition channel for O<sub>2</sub> molecules to jump from one hole to another, and then O<sub>2</sub> molecules overcome the energy barrier along the path to enter another hole. This is consistent with the mechanism of small-molecule diffusion in polymers<sup>[22]</sup>.

In contrast, the O<sub>2</sub> solubility of PF-y-P binders increases with increasing phosphonic acidification; in particular, the O<sub>2</sub> solubility of PF-1-P binder materials can be as high as  $5.36 \times 10^{-6} \text{ mol cm}^{-3}$ , which may be due to the strong intermolecular forces generated by the tetrafluorophenyl phosphonic acid group that cause the polymer to form more micropores. According to the dual-mode model, the microvoids (or “cage”) in the membrane immobilize O<sub>2</sub> molecules by entrapment or binding to high-

energy sites at the molecular periphery of the micropore, allowing oxygen to dissolve in the membrane (similar to adsorption)<sup>[23]</sup>.

During ORR at the cathode, oxygen transport is required to traverse the void space within the cathode CL. However, binder molecules tend to accumulate and cover the catalyst surface, potentially blocking the pores between the carbon carriers, a phenomenon that adversely affects oxygen penetration. On the one hand, the more numerous and complex microporous structure of PF-1-P provides more space for O<sub>2</sub> retention (solubility), and at the same time, more water is retained due to capillary forces. However, the complex pore structure is not favorable for oxygen diffusion. This in turn leads to a decrease in oxygen permeability. Therefore, finding a proper balance between the oxygen diffusion coefficient and solubility is crucial for the efficient construction of a three-phase interface within the HT-PEMFC cathode CL.

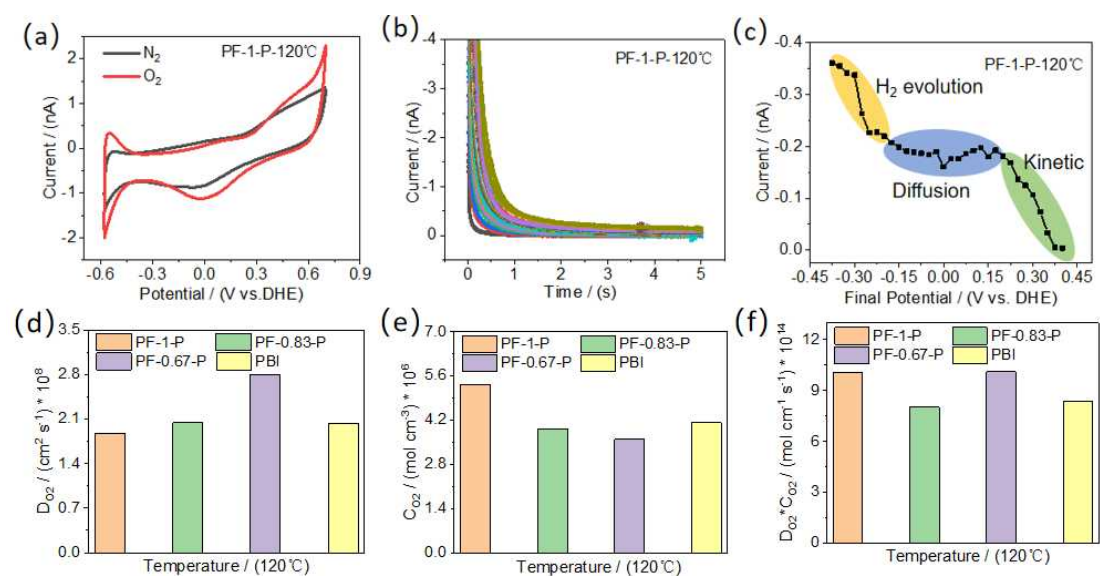


**Fig. 4.** (a) Cyclic voltammograms obtained at a scan rate of 250 mV s<sup>-1</sup> in N<sub>2</sub> and O<sub>2</sub> atmospheres, (b) potential-step chronoamperometry curves, (c) voltammograms obtained by sampling current

from (b) at 2 s, (d) diffusion coefficient ( $D_{O_2}$ ) of PF-y-P and PBI at 120°C, (e) solubility ( $C_{O_2}$ ) of PF-y-P and PBI at 120°C, and (f) permeability ( $D_{O_2} * C_{O_2}$ ) of PF-y-P and PBI at 120°C

**Table 4**  $D_{O_2}$ ,  $C_{O_2}$  and  $D_{O_2} * C_{O_2}$  of PF-y-P and PBI

	PF-1-P	PF-0.83-P	PF-0.67-P	PBI
$D_{O_2} / (\text{cm}^2 \text{ s}^{-1})$	1.88E-8	2.04E-8	2.8E-8	2.03E-8
$C_{O_2} (\text{mol cm}^{-3})$	5.34E-6	3.93E-6	3.6E-6	4.12E-6
$D_{O_2} * C_{O_2} / (\text{mol cm}^{-1} \text{ s}^{-1})$	1.01E-13	8.02E-14	1.01E-13	8.36E-14

Fig. 5(a) shows the polarization curves and power densities of the single cells tested at 120°C humidified conditions using PF-1-P, PF-0.83-P, and PF-0.67-P as catalyst binders. The open-circuit voltages of the PF-y-P-type materials used as binders for MEA range from 0.83 V to 0.86 V, with little difference. Peak power densities of PF-1-P, PF-0.83-P, and PF-0.67-P are  $0.161 \text{ W cm}^{-2}$ ,  $0.137 \text{ W cm}^{-2}$ , and  $0.118 \text{ W cm}^{-2}$ , respectively, and show a sequential increasing trend with the increasing degree of phosphonation. This can be attributed to the fact that the higher the degree of phosphonation, the greater the proton conductivity of the material, and the higher proton conductivity is conducive to the formation of the three-phase interface of the catalytic active center, which promotes the electrocatalytic reaction. In particular, PF-1-y exhibits superior performance, further implying that the PF-1-y catalyst binder is more favorable for oxygen transport in the CL of the assembled cell. This agrees with our reference to the dense tetrafluorophenyl phosphonic acid moiety of PF-1-y, whose interacting forces allow PF-1-y to possess a better balance in solubility and diffusion coefficient. In addition, from the surface morphology of the catalytic layer, it can be

found that the degree of fracture of the catalytic layer decreases with increasing the phosphonation degree of the PF-y-P-type materials and the degree of fracture of the surface morphology of the catalytic layer also affects the utilization efficiency of the Pt/C catalysts.

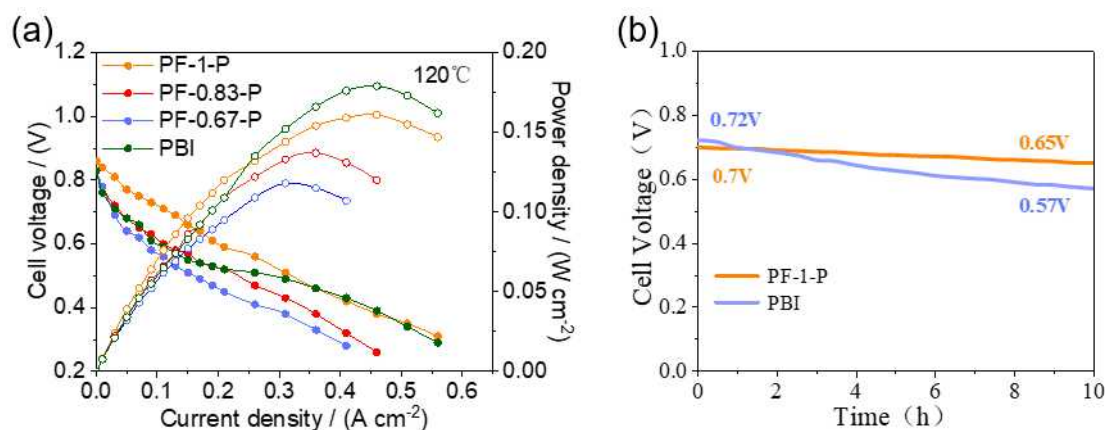


**Fig. 5.** (a) Power density and polarization curves of PF-y-P and PBI binders under 120°C, H<sub>2</sub> and O<sub>2</sub> flow of 500 cm<sup>3</sup> min<sup>-1</sup>, and humidification conditions; (b) MEA stability test of PF-1-P and PBI as binder at 90°C, H<sub>2</sub> and O<sub>2</sub> flow 500 cm<sup>3</sup> min<sup>-1</sup>, and current density of 0.12 A cm<sup>-2</sup>

Fig. 5(b) shows that after 10.5 h of discharge at a constant current of 0.12 A cm<sup>-2</sup>, the voltage of the MEA containing PF-1-P binder decreased from 0.70 V to 0.65 V, which is a decrease of 7.1%, while the voltage of the MEA prepared by selecting the PBI material as binder decreased from 0.72 V to 0.57 V, which is a decrease of 20.8%. This indicates that the use of PF-1-P material as a binder has better single-cell stability than the use of PBI binder during long-term operation and is more promising for HT-PEMFC with PA-doped HT-PEM. The results described in this work suggest that tetrafluorophenyl phosphonic acid binders may be promising candidates as catalyst

binders in the CL of fuel cells.

### 3. Conclusions

In summary, for the problem of oxygen transport channel blockage by PA loss in the catalytic layer of HT-PEMFC, a series of tetrafluorophenyl phosphonic acid-based binder materials (PF-y-P,  $y = 1, 0.83, 0.67$ ) with controlled phosphonation degree were prepared by super acid-catalyzed Friedel-Crafts reaction between aldehydes, ketones, and biphenyls containing pentafluorophenyl and combined with Michaelis-Arbuzov reaction. Among them, the PF-0.67-P material has lower water absorption (2.3%) and higher dimensional swelling (2.5%), which is superior to that of PF-1-P material (5.8% and 7.6%). The water absorption and swelling of the PF-y-P material increase with temperature. The oxygen mass transport properties of the binder materials were investigated using high-temperature microelectrode electrochemical testing techniques. The  $O_2$  solubility of PF-y-P binders increases with the degree of phosphonate acidification; in particular, the  $O_2$  solubility of PF-1-P binder materials can be as high as  $5.36 \times 10^{-6} \text{ mol cm}^{-3}$ , which is 30% higher than that of the PA-doped PBI binders ( $4.12 \times 10^{-6} \text{ mol cm}^{-3}$ ). This high  $O_2$  mass transport is beneficial for the continuous and timely transfer of  $O_2$  to the three-phase interface where the oxygen reduction electrochemical reaction occurs. In addition, Pt/C catalyst using PF-y-P as catalyst binder exhibited promising electrochemical stability. After 10.5 h of discharge at a constant current of  $0.12 \text{ A cm}^{-2}$ , the voltage of the MEA containing the PF-1-P binder decreased by 7.1%, while that of the PBI material as the binder decreased by 20.8%.

Thus, the results of assembled high-temperature proton-exchange membrane fuel cells demonstrate that phosphonic acid functionalization effectively avoids the problems of CL micropore blockage caused by doping with PA, which affects O<sub>2</sub> mass transfer.

#### 4. Experimental Section

**Preparation of the PF-y polymer:** The experimental procedure for PF-y preparation was described as follows: First, 10 mmol of pTP was taken in a flask and degassed three times with N<sub>2</sub> evacuation, 15 mL of DCM and 10.5 mmol of PFBf were added to the flask, and then N<sub>2</sub> was added at a speed of 400 rpm and kept on for 0.5 h. The suspension was then cooled to 0°C in an ice bath, and 20 mmol of TFSA was added dropwise. After the dropwise addition, the reaction solution was kept at 0°C for 0.5 h and then gradually brought to room temperature and reacted at this temperature for 48 h. The reaction solution became very viscous to the point that the rotor could hardly turn. The reaction was then quenched by the addition of 15 mL of DCM, and the reaction product was diluted. The reaction solution was slowly poured into methanol solution for precipitation, and the resulting polymer PF-1 was filtered and dried in a vacuum oven at 60°C for 12 h. Based on 10 mmol of pTP monomer, the amounts of PFBf and TFAP used to synthesize copolymer PF-0.83 were 9 mmol and 3 mmol, respectively, and the amounts of PFBf and TFAP used to synthesize copolymer PF 0.67 were 7 mmol and 5 mmol, respectively.

**Preparation of phosphonated PF-y-P:** Take the synthesis of PF-1-P as an example to describe the corresponding experimental steps: First, 1 g of PF-1 was added into the

flask and subjected to vacuum degassing and dehydration three times, 12 mL of NMP was added into the flask, and the temperature was raised to 90°C so that the PF-1 was completely dissolved, and then 10 mL of TSP was added one by one after the temperature was raised to 180°C to keep the reaction lasting for 14 h. The reaction solution was then reduced to room temperature and slowly poured into 350 mL of deionized water for precipitation. The light-red precipitate of trimethylsilyl phosphonate was washed several times, and the filtered material was treated with HCl at 50°C for 24 h, filtered to obtain a burgundy solid, washed several times, and then dried under vacuum at 50°C for 24 h. Finally, the phosphonated PF-1-P was obtained, and PF-0.83-P and PF-0.67-P were prepared by the same manner.

**Microelectrode characterizations:** The O<sub>2</sub> mass transport properties of PF-y-P class binder and PBI binder materials were tested by a home-built microelectrode device (Fig. 6) at 120°C. In general, the binder samples were first cast into 3 cm × 3 cm films and placed evenly on the counter electrode. A platinum wire (25 μm in diameter) microelectrode served as the working electrode to connect to the other side of the films. A sampling current method with more details shown in the Supporting Information was applied to obtain O<sub>2</sub> diffusion coefficient and solubility parameters.

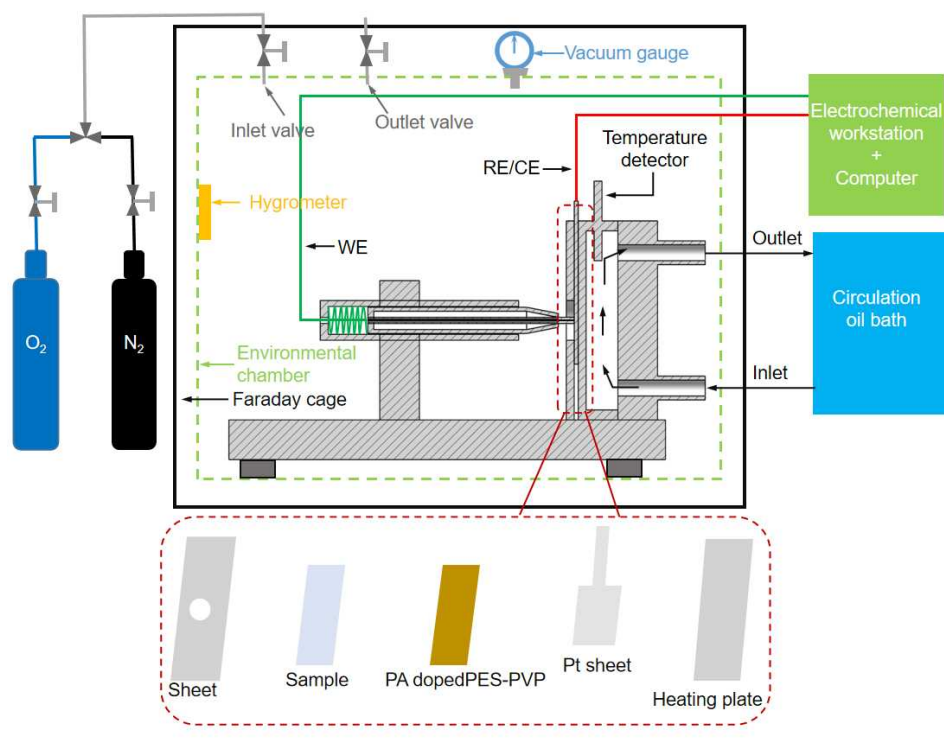


**Fig. 6** Schematic illustration of microelectrode device used for testing oxygen mass transfer of thin membranes

**Fuel cell testing:** HT-PEMFC single cells were assembled using PF-y-P as binder in catalyst layers, commercial Pt/C as the catalyst in both anode and cathode, and commercial PBI doped with  $\text{H}_3\text{PO}_4$  as membrane electrolyte. To test the cell operation stability of PF-1-P and PBI binders, the PA loss and MEA aging in HT-PEM membranes were accelerated by subjecting the single cell to a constant current discharge mode at  $90^\circ\text{C}$ , a flow rate of  $500\text{ cm}^3\text{ min}^{-1}$  for both  $\text{H}_2$  and  $\text{O}_2$ , a current density of  $0.12\text{ A cm}^{-2}$ , and high humidity conditions in which both  $\text{H}_2$  and  $\text{O}_2$  were humidified prior to being passed through the single cell.

## Supporting Information

More experimental section and methods including the structural characterization, thermal and chemical stability testing, water absorption, dimensional solubility and hydrophilicity testing, proton conductivity tests, O<sub>2</sub> mass transfer models can be found in the Supporting Information.

### **Acknowledgements**

The authors gratefully acknowledge the financial support from the National Natural Science Foundation of China (No. 22178307) and China Southern Power Grid (Grant Nos. 0470002022030103HX00002-01).

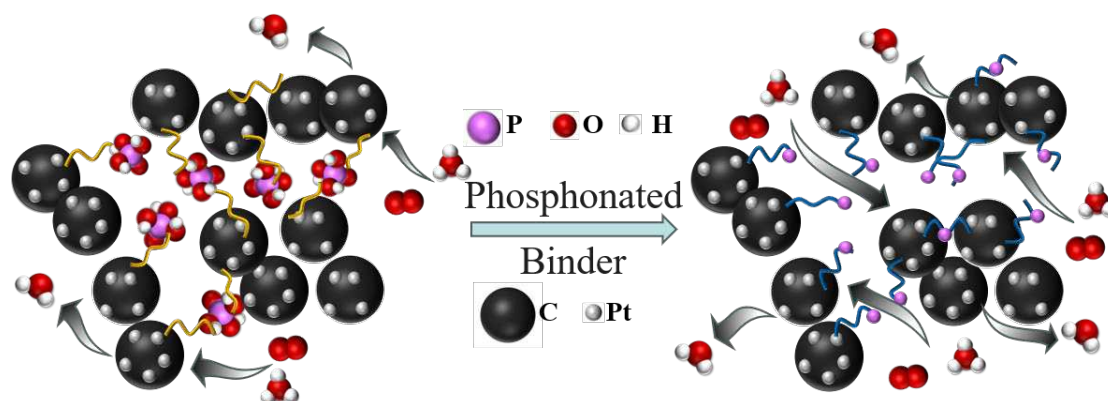
## References

- [1] G. G. Eshetu, M. Armand, H. Ohno, B. Scrosati, S. Passerini, *Energy & Environmental Science* **2016**, *9*, 49-61.
- [2] M. A. Haque, A. B. Sulong, K. S. Loh, E. H. Majlan, T. Husaini, R. E. Rosli, *International Journal of Hydrogen Energy* **2017**, *42*, 9156-9179.
- [3] <sup>a</sup>A. Parthasarthy, S. Srinivasan, A. J. Appleby, C. R. Martin, *Journal of Electroanalytical Chemistry* **1992**, *339*, 101-121; <sup>b</sup>S. S. Araya, F. Zhou, V. Liso, S. L. Sahlin, J. R. Vang, S. Thomas, X. Gao, C. Jeppesen, S. K. Kaer, *International Journal of Hydrogen Energy* **2016**, *41*, 21310-21344; <sup>c</sup>Y. Z. Hu, T. Shen, X. R. Zhao, J. J. Zhang, Y. Lu, J. Shen, S. F. Lu, Z. K. Tu, H. L. L. Xin, D. L. Wang, *Applied Catalysis B-Environmental* **2020**, *279*, 8; <sup>d</sup>R. Haider, Y. C. Wen, Z. F. Ma, D. P. Wilkinson, L. Zhang, X. X. Yuan, S. Q. Song, J. J. Zhang, *Chemical Society reviews* **2021**, *50*, 1138-1187; <sup>e</sup>D. W. Shin, M. D. Guiver, Y. M. Lee, *Chemical Reviews* **2017**, *117*, 4759-4805; <sup>f</sup>J. Lin, J. Wang, Y. Wu, P. Yang, Q. Liu, M. Li, S. Du, R. Chen, L. Tao, **2023**, *18*, e202300137; <sup>g</sup>S. Mo, L. Du, Z. Huang, J. Chen, Y. Zhou, P. Wu, L. Meng, N. Wang, L. Xing, M. Zhao, Y. Yang, J. Tang, Y. Zou, S. Ye, *Electrochemical Energy Reviews* **2023**, *6*, 28.
- [4] <sup>a</sup>K. Jin, B. Yue, L. Yan, R. Qiao, H. Zhao, J. Zhang, **2022**, *17*, e202200109; <sup>b</sup>A. Zucconi, J. Hack, R. Stocker, T. A. M. Suter, A. J. E. Rettie, D. J. L. Brett, *Journal of Materials Chemistry A* **2024**, *12*, 8014-8064; <sup>c</sup>Q. Meyer, C. Yang, Y. Cheng, C. Zhao, *Electrochemical Energy Reviews* **2023**, *6*, 16.
- [5] L. Chong, J. G. Wen, J. Kubal, F. G. Sen, J. X. Zou, J. Greeley, M. Chan, H. Barkholtz, W. J. Ding, D. J. Liu, *Science* **2018**, *362*, 1276-+.

- [6] J. F. Zhang, W. K. Zhu, T. Huang, C. Y. Zheng, Y. B. A. Pei, G. Q. Shen, Z. X. Nie, D. Xiao, Y. Yin, M. D. Guiver, *Advanced Science* **2021**, *8*, 26.
- [7] <sup>a</sup>M. S. Wilson, S. Gottesfeld, *Journal of Applied Electrochemistry* **1992**, *22*, 1-7; <sup>b</sup>L. Q. Wang, E. Magliocca, E. L. Cunningham, W. E. Mustain, S. D. Poynton, R. Escudero-Cid, M. M. Nasef, J. Ponce-Gonzalez, R. Bance-Souahli, R. C. T. Slade, D. K. Whelligan, J. R. Varcoe, *Green Chemistry* **2017**, *19*, 831-843.
- [8] <sup>a</sup>H. N. Su, S. Pasupathi, B. Bladergroen, V. Linkov, B. G. Pollet, *International Journal of Hydrogen Energy* **2013**, *38*, 11370-11378; <sup>b</sup>D. Kim, H. S. Jung, H. Chun, C. Pak, *International Journal of Hydrogen Energy* **2021**, *46*, 29424-29431; <sup>c</sup>F. Mack, T. Morawietz, R. Hiesgen, D. Kramer, R. Zeis, in *13th Polymer Electrolyte Fuel Cell Symposium (PEFC)*, Vol. 58, Electrochemical Soc Inc, San Francisco, CA, **2013**, pp. 881-888.
- [9] F. Mack, T. Morawietz, R. Hiesgen, D. Kramer, V. Gogel, R. Zeis, *International Journal of Hydrogen Energy* **2016**, *41*, 7475-7483.
- [10] S. Kim, T. D. Myles, H. R. Kunz, D. Kwak, Y. Wang, R. Maric, *Electrochimica Acta* **2015**, *177*, 190-200.
- [11] <sup>a</sup>R. Zeis, *Beilstein Journal of Nanotechnology* **2015**, *6*, 68-83; <sup>b</sup>S. Martin, Q. Li, J. O. Jensen, *Journal of Power Sources* **2015**, *293*, 51-56; <sup>c</sup>S. W. Choi, J. O. Park, C. Pak, K. H. Choi, J. C. Lee, H. Chang, *Polymers* **2013**, *5*, 77-111; <sup>d</sup>Y. Devrim, G. N. Bulanık Durmuş, *International Journal of Hydrogen Energy* **2022**, *47*, 9004-9017; <sup>e</sup>S. Diaz-Abad, S. Fernandez-Mancebo, M. A. Rodrigo, J. Lobato, *Membranes* **2022**, *12*, 13.
- [12] S. Zhang, J. Zhang, Z. Zhu, P. Liu, F. Cao, J. Chen, Q. He, M. Dou, S. Nan, S. Lu, *Journal*

- of Power Sources* **2020**, *473*, 228616.
- [13] S. Chen, J. Niu, S. Zhang, Z. Ma, Q. Zhang, S. Chen, L. Wu, J. Zhang, M. Wang, S. Lu, Q. He, *Journal of The Electrochemical Society* **2023**, *170*.
- [14] <sup>a</sup>A. Sannigrahi, S. Takamuku, P. Jannasch, *Polymer Chemistry* **2013**, *4*, 4207-4218; <sup>b</sup>E. Abouzari-Lotf, H. Ghassemi, A. Shockravi, T. Zawodzinski, D. Schiraldi, *Polymer* **2011**, *52*, 4709-4717; <sup>c</sup>H. Y. Tang, K. Geng, Y. X. Hu, N. W. Li, *Journal of Membrane Science* **2020**, *605*, 9.
- [15] V. Atanasov, A. S. Lee, E. J. Park, S. Maurya, E. D. Baca, C. Fujimoto, M. Hibbs, I. Matanovic, J. Kerres, Y. S. Kim, *Nature Materials* **2021**, *20*, 370-+.
- [16] R. Ren, S. Zhang, H. A. Miller, F. Vizza, J. R. Varcoe, Q. He, *Journal of Membrane Science* **2019**, *591*, 117320.
- [17] J. Niu, S. Zhang, Y. Li, X. Li, J. Zhang, S. Lu, Q. He, *Polymer* **2023**, *273*.
- [18] K. Akizuki, A. Ohma, S. Miura, T. Matsuura, M. Yoshizawa-Fujita, Y. Takeoka, M. Rikukawa, *Sustainable Energy & Fuels* **2017**, *1*, 1299-1302.
- [19] R. Ren, S. Zhang, H. A. Miller, F. Vizza, J. R. Varcoe, Q. He, *ACS Applied Energy Materials* **2019**, *2*, 4576-4581.
- [20] R. Haider, Y. Wen, Z. F. Ma, D. P. Wilkinson, L. Zhang, X. Yuan, S. Song, J. Zhang, *Chemical Society reviews* **2021**, *50*, 1138-1187.
- [21] T. G. Fox, P. J. Flory, **1954**, *14*, 315-319.
- [22] S. G. Charati, S. A. Stern, *Macromolecules* **1998**, *31*, 5529-5535.
- [23] H. L. Frisch, *Polymer Journal* **1991**, *23*, 445-456.

## Entry for the Table of Contents



Tetrafluorophenyl phosphonic acid binder shows high thermal stability, chemical stability, proton conductivity and oxygen mass transfer properties, which demonstrates its powerful ability as a binder material for high-temperature proton exchange membrane fuel cells.